

Experimental and Theoretical Study on Crack Growth Characteristics of the Full Size Partial Penetration Welded Nozzle

Y. Sakaguchi, T. Shindo, M. Kubo, T. Katori, S. Kimura

*Kure Works of Babcock-Hitachi K.K.,
6-9 Takara-Machi, Kure-City, Hiroshima, Japan*

Summary

This paper describes the results of full size fatigue testing of partial penetration welded nozzles attached to the spherical bottom head of the BWR reactor pressure vessel. In nozzles of this type the nozzle seating below the nozzle/wall weld is not welded, resulting in a notch-like opening in that region. Therefore, confirmation of structural integrity with regard to fatigue damage (crack initiation and crack propagation) is essential.

The test models were full size stub tubes which were welded (partial penetration) to a thick circular plate by production welding procedures using production welding material. The number of cycles to crack initiation and the crack propagation rate of weld metal were calculated using data from inspection of the fracture surface striation by a scanning electron microscope (SEM), and then the low cycle fatigue strength was evaluated. Furthermore, the crack propagation direction and the crack propagation rate were determined by fracture mechanics and compared with the experimental results.

After the verification of the crack propagation analysis by comparison with the experimental results, the fatigue strength of a production asymmetric partial penetration welded nozzle was evaluated. The stresses of an asymmetric nozzle were obtained by correcting the stresses of a two-dimensional axisymmetric nozzle using asymmetric stress factors which were obtained from 3-D FEM stress analysis.

The following results were obtained:

- (1) The crack propagation direction determined by the stiffness derivative procedure using FEM analysis, was in good agreement with the experimental results.
- (2) The relationship between the fatigue crack propagation rate (da/dN) obtained from the experimental results and the range of stress intensity factor (ΔK) obtained from the stiffness derivative procedure was in good agreement with the relationship of $da/dN \sim \Delta K$ which was obtained from the crack propagation test of the weld metal.
- (3) The number of cycles to crack initiation of the weld metal was evaluated. The low cycle fatigue strength and the structural integrity of a production partial penetration welded nozzle were confirmed to be sufficient.

1. INTRODUCTION

In the reactor pressure vessel several partial penetration welded type nozzles are used. In nozzles of this type the nozzle seating below the nozzle/weld is not welded, resulting in a notch-like opening in that region. Therefore, confirmation of structural integrity with regard to fatigue damage (crack initiation and crack propagation) is essential.

This paper describes the results of the stress and fatigue evaluation of partial penetration welded nozzles (internal stub tubes with control rod hydraulic drive system penetrations, usually abbreviated to "CRD stubs", however hereinafter referred to as "nozzles") attached to the spherical head of the BWR reactor pressure vessel.

The following items have been examined.

- (1) Full size model fatigue testing and measurement of crack initiation and crack propagation
- (2) Estimation of crack propagation direction and crack propagation rate, using the stiffness derivative procedure, and comparison with experimental results
- (3) Stress analysis of a production asymmetric partial penetration welded nozzle using 3-D finite element method (FEM)
- (4) Evaluation of crack initiation and crack propagation of a production asymmetric partial penetration welded nozzle

2. FULL SIZE FATIGUE TESTING

The arrangement and the structure of partial penetration welded nozzles are shown in Fig. 1 and Fig. 2. The nozzles are attached to the spherical bottom head parallel to the center axis as shown in Fig. 1. Therefore, the nozzles which are distributed over the bottom head off the center axis are asymmetric, maximum outside oblique angle 46 degrees. The full size fatigue test models were limited to axisymmetric nozzles, however the effect of asymmetry is described in chap. 4.

2.1. TEST MODELS

The shapes and the dimensions of the test models are shown in Fig. 3. In the production nozzles the stresses are dominantly generated by the radial expansion displacement of the bottom head due to internal pressure or thermal transients, resulting in the opening of the notch region. However, it was impossible to reproduce the same distribution in the test model on account of the limitation of the testing machine.

The test models were full size stub tubes which were welded (partial penetration) to a thick circular plate by production welding procedures and welding material. The cyclic opening of the notch was achieved by using a special jig to provide the notch opening mode load by converting the compression load of the testing machine to a bending load.

Three test models (A,B,C) were fabricated. Test models A and B were loose fit nozzles, the outside diameters of the stubs being a little smaller than the hole diameters of the circular plates. Conversely, in test model C the former was a little larger than the latter, and the stub tube was set in to the circular plate after being cooled and shrunk by liquid nitrogen. The stub tube had an interference fit with the plate at room temperature in this model. A 300ton MTS fatigue testing machine was used for these tests. A general view of the loading method is shown in Fig. 4. The cyclic compression load was applied to the plate around the stub through load guides.

Because it was impossible to verify and measure the crack initiation and propagation visually, the crack propagation was monitored by an ultrasonic flaw detector using a focus type probe.

2.2. EXPERIMENTAL RESULTS

A photograph of the test model section with the crack dyed by liquid penetrant is shown in Fig. 5. The crack propagated through the weld metal in a direction inclined at an angle of 24~30 degrees to the center axis of the stub.

The circumferential distribution of the crack length was almost uniform. It was found as a result of observation of the microscopic structure near the crack route by a optical microscope that the crack propagated intergranulary and had few branches.

Photographs of the fracture surfaces of the test model for the purpose of the observation of macroscopic structure after pulling apart are shown in Fig. 6. The trails which are visible on the fracture surface are beach marks created by cyclic loads between 50% load and full load which were applied at intervals.

Fig. 7 shows the fracture surfaces, photographed using a scanning electron microscope, in which striation is visible distinctly. The more the crack grows, the wider the striation becomes.

As the striation (S) is generally considered to be equal to the crack propagation rate (da/dN) in steel, the relationship between the striation and the depth of the crack is difined by eq. (1) using logarithmic rectilinear approximation in each test model.

$$S = da/dN = A \cdot a^m \quad (1)$$

where, a is the crack length measured from the bottom surface of the test model, and A and m are constants.

The crack initiation life of each model has been estimated by integrating eq.(1) and is shown in Fig. 13. The test models A and C were tested at the same load level to examine the effectiveness of the interference fit. However, the crack initiation life in test model C was shorter than that in test model A. Therefore, it was found that initial pre-stresses of an interference fit were ineffective within the limit of this test.

3. CRACK PROPAGATION ANALYSIS USING STIFFNESS DERIVATIVE PROCEDURE

The finite element method was used to determine elastic stress intensity factors and analyze the crack propagation rate and propagation direction.

The energy release rate (G) is defined as the potential energy decrease per unit crack advance. [1, 2]

$$G = - \frac{\Delta P}{\Delta l} \quad (2)$$

$G(\varphi)$ is also defined as the potential energy release rate when the crack would propagate at an angle φ .

$$G(\varphi) = - \frac{\Delta P(\varphi)}{\Delta l} \quad (3)$$

$G(\varphi)$ is calculated from the increase of the sum of each element strain energy which results from the small crack advance near the crack tip by releasing the combination of the fine mesh elements in the direction φ . (See Fig. 8)

The mesh configurations used in the analysis are shown in Fig. 9. Three cases where the

crack propagation length is 0mm, 5mm, 10mm respectively and the crack direction is at an angle of 24 degrees to the center axis were analyzed. The $G(\varphi)$ distribution of the crack tip for each case is shown in Fig. 10.

The $G(\varphi)$ values on the weld metal side (outside) are larger than that on the stub side (inside). This tendency increases a little with the crack advance. These results are in good agreement with the experimental results.

When the direction, φ , coincides with the direction of previous crack advance, the relationship between $G(\varphi_0)$ and the stress intensity factor (K_I) is described by eq. (4). (2)

$$\Delta K_I \equiv K_I = \sqrt{\frac{E \cdot G(\varphi_0)}{1 - \nu^2}} \quad (4)$$

We may deduce the fatigue crack propagation rate, corresponding with each crack length, by using the range of stress intensity factor, obtained from eq. (4), and the experimental relationship between the fatigue crack propagation rate and the range of stress intensity factor of the weld metal, as shown in Fig. 11 (a). The fatigue crack propagation rate derived by the analysis was in good agreement with the fatigue crack propagation rate determined from the actual crack length, which was obtained from the striation on the fracture surface in the test model, as shown in Fig. 11 (b).

4. STRESS ANALYSIS OF AN ASYMMETRIC NOZZLE USING 3-D FEM MODEL

4.1. METHOD OF ANALYSIS

As the production nozzles are mostly asymmetric as shown in Fig. 1 and Fig. 2, it is necessary to grasp the effect of asymmetry. A single asymmetric nozzle has been modeled by 3-D FEM using the mesh configuration shown in Fig. 12.

Stress analysis has been carried out not only on an asymmetric nozzle but on an axisymmetric nozzle subjected to mechanical loads and thermal transients using the same mesh pattern to examine the effect of asymmetry. The MARC finite element program was used for these analyses.

4.2. ASYMMETRIC STRESS FACTORS

After the implementation of the analysis, the difference of stresses due to the structural difference between an asymmetric nozzle and an axisymmetric one has been settled using asymmetric stress factors which are defined by eq. (5).

$$\alpha(i, j, k, l) = \frac{\sigma_1(i, j, k, l)}{\sigma_0(i, j, k, l)} \quad (5)$$

where, α : asymmetric stress factors

σ_0 : stresses of an axisymmetric nozzle

σ_1 : stresses of an asymmetric nozzle (oblique angle = 46 degrees)

i : subscript of evaluation location

j : subscript of classification of loading type

k : subscript of classification of stress type

l : subscript of stress component

The asymmetric stress factors which were obtained for each loading condition are shown in Table 1. It can be seen from Table 1 that the asymmetric stress factors do not have the same value and they depend intricately on the loading type, the stress type and the stress

component. We may deduce the stresses of an asymmetric nozzle using the asymmetric stress factors and the analysis of an axisymmetric nozzle, without the 3-D FEM structural analysis which is costly.

5. CRACK INITIATION & CRACK PROPAGATION EVALUATION OF A PRODUCTION PARTIAL PENETRATION NOZZLE

5.1. EVALUATION OF CRACK INITIATION

The fatigue usage factors for crack initiation at the notch of the asymmetric nozzle were calculated according to the ASME Code fatigue design procedure [3], using the lower bound fatigue strength curve for crack initiation derived from experimental data, and are shown in Table 2.

In the calculation of the stresses the asymmetric stress factors which are given in chap. 4 and the fatigue strength reduction factor, 5, which is the maximum value prescribed in Japanese Standards [4] for a local structural discontinuity (of course satisfactory to the ASME Code) were used.

The lower bound fatigue curve used in the evaluation is shown in Fig. 13, which was obtained from the experimental results of the sliced model of the partial penetration welded nozzles by Kusumoto et al. [5] and of the axisymmetric models described in chap. 2. As shown in Table 2, the integrity for crack initiation of the notch of the asymmetric nozzles was confirmed.

5.2 EVALUATION OF CRACK PROPAGATION

The $G(\varphi)$ distribution of the notch on each loading condition of the RPV is shown in Fig. 14. The $G(\varphi)$ values of other loading conditions, which are not shown in Fig. 14, were all negative. In each loading condition $G(\varphi)$ had the maximum value at $\varphi = 0^\circ$, therefore it is considered that the crack would propagate straight ahead.

The stress intensity factor (K_I) on each loading condition was obtained using eq. (4). The K_I value of a axisymmetric nozzle is calculated to be the maximum, $38.0 \text{ kg mm}^{-3/2}$, at the Code hydrostatic testing condition. In the evaluation of the asymmetric nozzle, since the stress intensity factor is in proportion to the nominal stress, we may use the K_I value, $42.6 \text{ kg mm}^{-3/2}$, multiplied by the asymmetric stress factor, 1.12, shown in chap. 4, which was selected as the maximum asymmetric stress factor for crack opening stress components, σ_1 , of internal pressure and thermal transients which caused dominant stresses of the nozzle.

The threshold of stress intensity factor for crack propagation (ΔK_{th}) was used in evaluation, in the case where we should consider the notch as being a crack tip in view of the shape of the nozzle. The relationship between the fatigue crack propagation rate (da/dN) and the range of stress intensity factor (ΔK) which was obtained from the fatigue crack propagation test of Inconel 600 at temperatures of 24°C and 316°C [6] is shown in Fig. 15. This figure shows that ΔK_{th} was about $60 \sim 70 \text{ kg mm}^{-3/2}$. It is concluded that the ΔK 's in all loading conditions were less than ΔK_{th} in the asymmetric nozzles.

6. CONCLUSION

The results are summarized as follows.

- (1) The crack propagation and the crack propagation rate determined by the stiffness

derivative procedure were in good agreement with the experimental results.

- (2) The number of cycles to crack initiation and the possibility of crack propagation of a production partial penetration welded nozzle were evaluated. The low cycle fatigue strength and structural integrity were confirmed to be sufficient.

REFERENCES

- [1] J. R. Rice, A Path Independent Integral and the Approximate Analysis of Strain Concentration by Notches and Cracks, Journal of Applied Mechanics, vol. 35 (1968) pp. 379-386
- [2] D. M. Parks, A stiffness derivative finite element technique for determination of crack tip stress intensity factors, International Journal of Fracture, vol. 10 (1974) pp. 487-502
- [3] ASME Boiler and Pressure Vessel Code Section III, Division 1, 1980 Edition
- [4] Notice Regarding Technical Standards for Structures, etc. for Power Generating Nuclear Facilities, Notice No. 501 of the Ministry of International Trade and Industry, 1980
- [5] S. Kusumoto and Y. Murakami, Low-Cycle Fatigue Strength of Nozzle-end Weldments for Reactor Pressure Vessel, the Hitachi Hyoron, vol. 51 (1969) pp. 72-76
- [6] L. A. James, Fatigue-Crack Propagation Behaviour of Inconel 600, International Journal of Pressure Vessel and Piping, vol. 5 (1977) pp. 241-259

TABLE 1 ASYMMETRIC STRESS FACTORS, $\alpha(i,j,k,l)$

LOADING TYPE, j	STRESS TYPE, k	STRESS COMPONENT, l	EVALUATION LOCATION, i			
			A		B	
			$\theta = 0^\circ$	$\theta = 180^\circ$	$\theta = 0^\circ$	$\theta = 180^\circ$
INTERNAL PRESSURE (P)	MEMBRANE	σ_t	0.89	1.42	0.68	1.31
		σ_l	0.65	-0.10	0.50	1.12
	BENDING	σ_t	-0.51	-2.01	1.15	3.18
		σ_l	1.19	-0.53	1.02	-0.06
VERTICAL MECHANICAL LOAD (V)	MEMBRANE	σ_t	-0.20	1.54	-0.64	0.43
		σ_l	0.27	0.42	-0.24	0.59
	BENDING	σ_t	2.50	-1.10	-0.89	1.17
		σ_l	3.38	1.13	-3.58	1.58
HORIZONTAL MECHANICAL LOAD (H)	MEMBRANE	σ_t	0.68	0.82	1.46	0.45
		σ_l	0.59	0.41	1.37	0.34
	BENDING	σ_t	1.45	2.09	1.48	0.62
		σ_l	1.54	-0.35	1.73	0.34
THERMAL LOAD AT STEADY STATE	MEMBRANE	σ_t	0.56	1.01	0.94	0.92
		σ_l	-0.11	0.16	0.49	0.72
	BENDING	σ_t	2.02	1.95	0.75	1.56
		σ_l	1.77	0.99	1.07	0.98
THERMAL LOAD AT COOLING DOWN	MEMBRANE	σ_t	0.59	1.42	0.67	1.25
		σ_l	0.39	2.48	0.67	1.06
	BENDING	σ_t	0.30	-1.82	1.17	0.79
		σ_l	1.01	-0.15	1.36	0.51

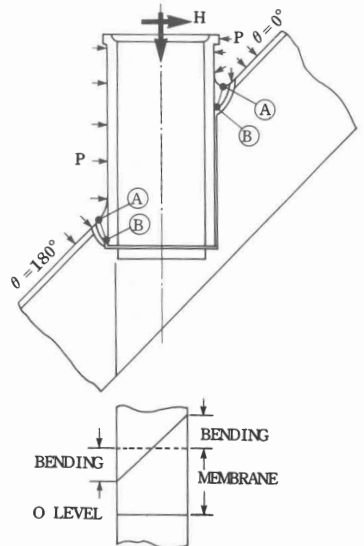


TABLE 2 CUMULATIVE USAGE FACTOR FOR FATIGUE CRACK INITIATION

EVALUATION LOCATION	CUMULATIVE USAGE FACTOR
(B) at $\theta = 0^\circ$	0.000 < 1.0
(B) at $\theta = 180^\circ$	0.380 < 1.0

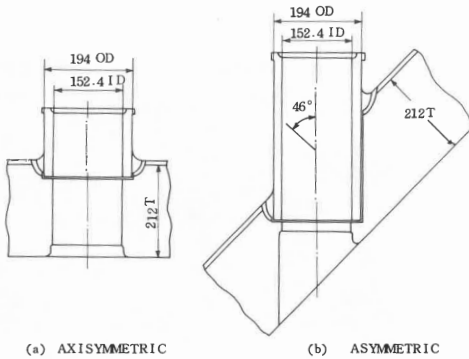


FIGURE 2 STRUCTURE OF CRD STUBS

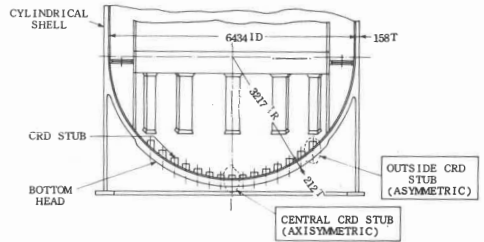


FIGURE 1 ARRANGEMENT OF CRD STUBS

①	circular thick plate (SA283D)
②	stub tube (SB 166)
③	surfacing weld metal (SFA-5.11ENiCrFe-2)
④	weld metal (SFA-5.11 ENiCrFe-2)

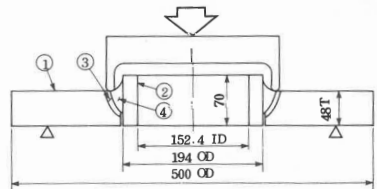
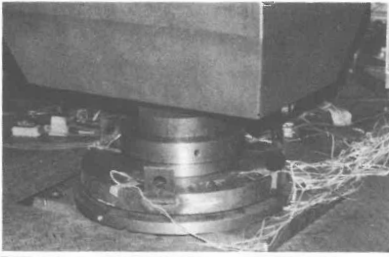


FIGURE 3 SHAPE OF TEST MODEL



RANGE OF COMPRESSION LOAD	TEST MODEL A	(0 ton ↔ 240 ton) 1.2Hz
	TEST MODEL B	(0 ton ↔ 192 ton) 1.5Hz
	TEST MODEL C	(0 ton ↔ 240 ton) 1.2Hz

FIGURE 4
GENERAL VIEW OF LOADING METHOD

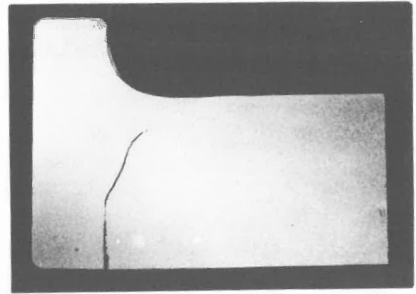


FIGURE 5 SECTION OF TEST MODEL AFTER CRACK PROPAGATION (TEST MODEL A)

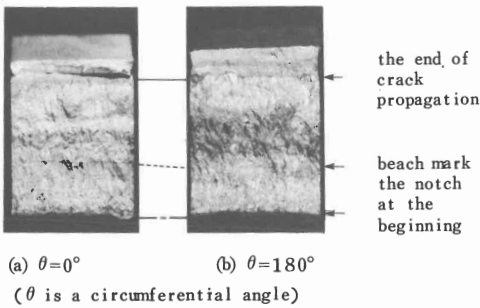


FIGURE 6 FRACTURE SURFACES OF TEST MODEL (TEST MODEL A)

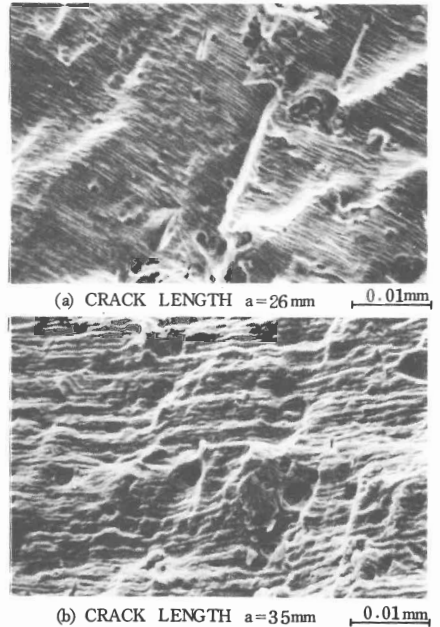


FIGURE 7 MICROSCOPIC FRACTURE SURFACES (TEST MODEL A)

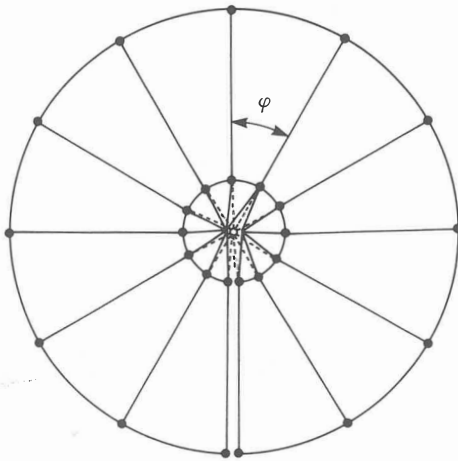
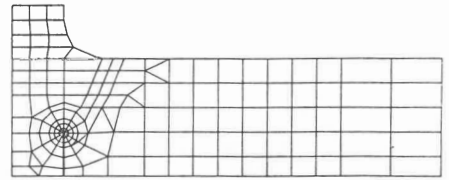
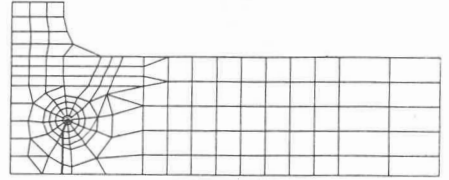


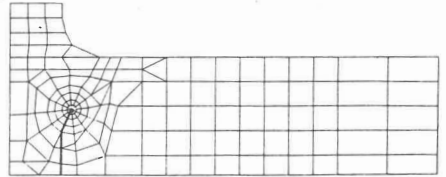
FIGURE 8 METHOD OF SMALL CRACK ADVANCE ON FEM MESH



(a) CRACK PROPAGATION LENGTH, $\Delta a = 0$ mm



(b) CRACK PROPAGATION LENGTH, $\Delta a = 5$ mm



(c) CRACK PROPAGATION LENGTH, $\Delta a = 10$ mm

FIGURE 9 MESH CONFIGURATIONS USED IN CRACK PROPAGATION ANALYSIS

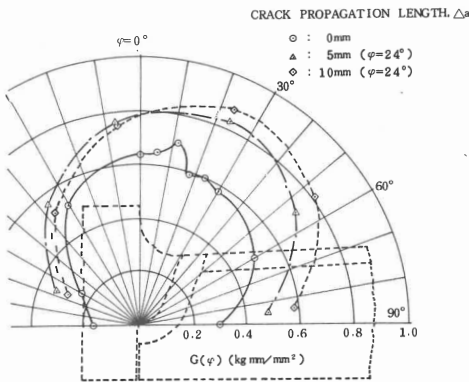


FIGURE 10 $G(\varphi)$ DISTRIBUTION OF TEST MODEL

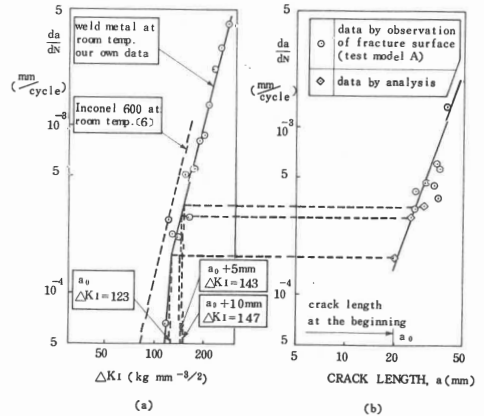


FIGURE 11 CRACK PROPAGATION RATE BY ANALYSIS COMPARED WITH THE DATA BY OBSERVATION OF FRACTURE SURFACE

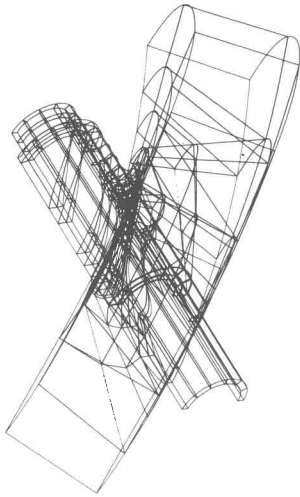


FIGURE 12 MESH CONFIGURATION USED IN 3-D FEM ANALYSIS

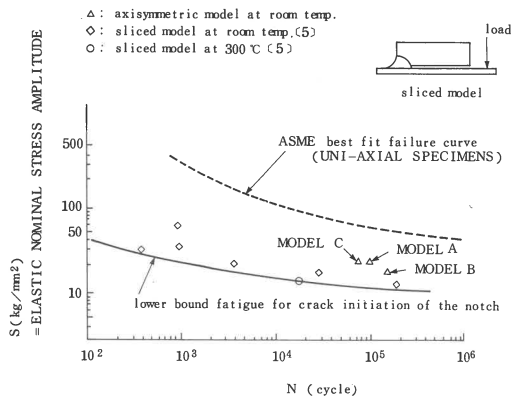


FIGURE 13 LOWER BOUND FATIGUE CURVE FOR CRACK INITIATION

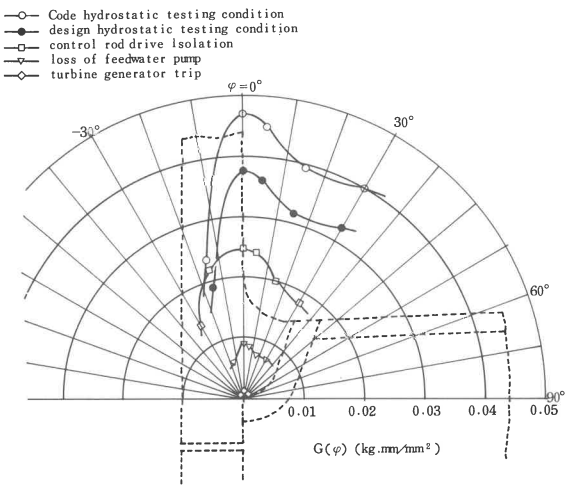


FIGURE 14 $G(\varphi)$ DISTRIBUTION OF PRODUCTION AXISYMMETRIC NOZZLE

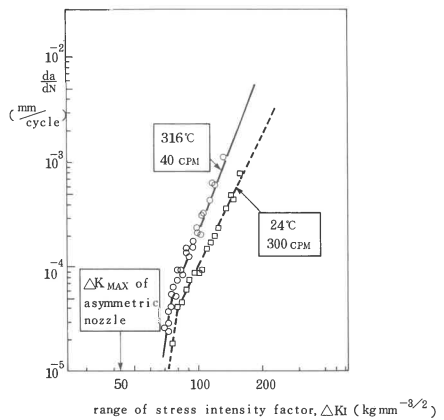


FIGURE 15 RELATIONSHIP BETWEEN THE RANGE OF STRESS INTENSITY FACTOR AND THE CRACK PROPAGATION RATE OF INCONEL 600